Actuator Grouping Optimization on Flexible Space Reflectors

Jeffrey R. Hill*[a], K. W. Wang[a], Houfei Fang[b], Ubaldo Quijano[b]
[a]University of Michigan, Department of Mechanical Engineering, Ann Arbor, MI, 48109, USA;
[b]Jet Propulsion Laboratory, California Institute of Technology, Pasadena, CA, 91109, USA

ABSTRACT

With the rapid advances in deployable membrane and mesh antenna technologies, the feasibility of developing large, lightweight reflectors has greatly improved. In order to achieve the required surface accuracy, precision surface control is needed on these lightweight reflectors. For this study, an analytical model is shown which combines a flexible Kapton reflector with Polyvinylidene fluoride (PVDF) actuators for surface control. Surface errors are introduced that are similar to real world scenarios, and a least squares control algorithm is developed for surface control. Experimental results on a 2.4 meter reflector show that while the analytical reflector model is generally correct, due to idiosyncrasies in the reflector it cannot be used for online control. A new method called the En Mass Elimination algorithm is used to determine the optimal grouping of actuators when the number of actuators in the system exceeds the number of power supplies available.

Keywords: Gossamar, shape control, EME algorithm, Grouping Optimization

1. INTRODUCTION

With the rapid advances in deployable membrane and mesh antenna technologies [1], the feasibility of developing large, lightweight reflectors has greatly improved. There are many benefits of using deployable membranes, such as reduced mass and stowage size thus allowing for a larger aperture, and a higher possible orbit. However, a major shortcoming of deployable membrane reflectors is the difficulty in maintaining a sufficiently tight surface accuracy.

The major problem is that in order to achieve high gain and low sidelobes, large deployable reflectors (5-35 meter diameter) operating at 14–35 GHz must keep a very tight surface tolerance: 0.54 mm (0.021 inches) at 14 GHz and 0.21 mm (0.008 inches) at 35 GHz. A surface tolerance of 0.21 mm is equivalent to the thickness of three sheets of paper. Studies have shown [2,3] that without any mechanisms to correct for mechanical and thermal distortion, a deployed reflector would nominally achieve a surface tolerance of 4.3 mm, which is 20 times the required surface accuracy.
In order to achieve the needed surface accuracy, high-precision surface control is needed. Past research has focused on a variety of control methods, such as using temperature gradients [4], boundary control [5,6], cable control [7-10], and domain control [11]. Domain control, where actuators are placed directly on the surface, has the ability to control more localized errors, but can require more actuators for control. Many studies to date have assumed that each actuator can be controlled individually. While ideally each actuator should be controlled by an individual power supply, sometimes it is realistically not feasible due to design, weight, or cost constraints. There are many instances where the only solution is to group multiple actuators together and power each group with a single power supply. For best performance, the grouping of actuators must be optimized. Some methods for actuator grouping that have been used are genetic algorithms [12-13] , circulant matrix theory [14], a recursive algorithm based on the Linear Quadratic Regulator [15] and a controllability Grammian method for open loop grouping [16]. Each of these approaches require the user to define a stop condition, and while these approaches indeed have merits, they lack the guarantee of a global optimal solution or even the guarantee of an acceptable solution.

The object of this research is to advance the state of the art and explore surface control and actuator grouping optimization utilizing a flexible Kapton reflector and Polyvinylidene fluoride (PVDF) actuators for surface control.

*jeffhill@umich.edu; phone 1 734 615-8747

2. REFLECTOR MODEL

A comprehensive reflector/actuator model has been developed to investigate surface control on an inflated flexible reflector using PVDF actuators. The primary cause of the surface error for this case is the thermal distortion due to the sun heating the reflector. The thermal loading is taken into account in the model, as well as pre-stress caused by the initial inflation of the membrane.

2.1 Reflector model

The reflector is modeled following the methodology proposed in [17], though a brief overview will be given here. The reflector is modeled as a thin shallow spherical cap [18]. The displacements (u, v and w) are defined relative to a spherical coordinate system, as shown in Figure 1, which coincides with the lines of principal curvature of the mid-surface.

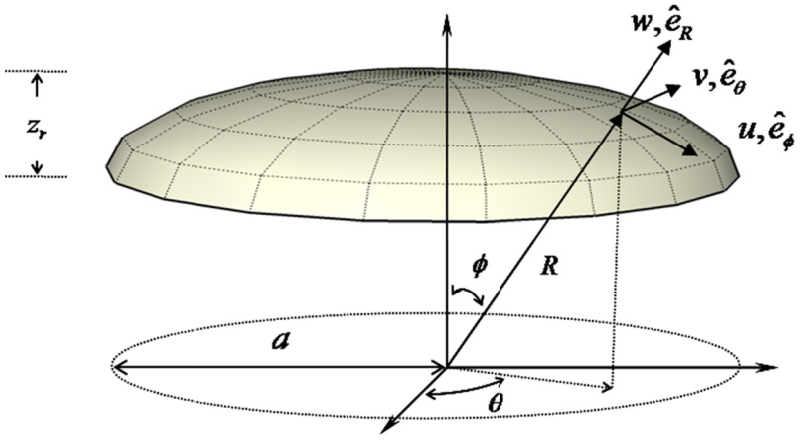

Figure 1 Reflector structural model: Spherical membrane cap with simply supported boundary conditions and pre-stress due to inflation.

Using the variation of energy functional and a Ritz method, the total reflector strain energy can be given by Eq. (1).

$$U_{ref} = \iiint_V \frac{1}{2}\{\sigma\}^T(\{\varepsilon\} - \{\varepsilon_T\})dV + \iiint_V \frac{1}{2}\sigma_{pre-stress}\left[\left(\frac{\partial w}{\partial r}\right)^2 + \left(\frac{1}{r}\frac{\partial w}{\partial \theta}\right)^2\right]dV \quad \textbf{(1)}$$

where σ is the stress in the reflector, ε is the strain, ε_T is the strain growth due to the thermal expansion of the material, and $\sigma_{pre-stress}$ is the stress induced by the inflation of the reflector.

Following the same method, the total energy for a single actuator can be given by Eq. (2)

$$U_{actuator_i} = \iiint_{V_i} \frac{1}{2}\{\sigma_a\}^T(\{\varepsilon_a\} - \{\varepsilon_E\})dV \quad \textbf{(2)}$$

where σ_a is the stress in each actuator, ε_a is the strain in each actuator, and ε_E represents the strain 'growth' due to the electric field placed on the PVDF material.

Assuming the reflector is a very thin shell, the displacements u and v of the reflector can be assumed to be varying linearly with the shell thickness, whereas the displacement w can be assumed to not vary at all with the shell thickness. The total energy of the reflector and actuator system is given by Eq. (3).

$$U_{total} = U_{ref} + \sum_i U_{actuator_i} \quad \textbf{(3)}$$

This system can be solved using the Ritz method, where the boundary conditions to be satisfied at the rim ($r = a$) and at the center ($r = 0$) of the reflector are

$$u_o(a,\theta) = v_o(a,\theta) = w_o(a,\theta) = u_o(0,\theta) = v_o(a,\theta) = 0. \quad \textbf{(4)}$$

A Fourier-Bessel series modal expansion that satisfy the boundary conditions is used, and the unknown Bessel coefficients can be grouped together into a single vector, $\{X\}$. Minimizing the total energy with respect to the unknown coefficients, a linear system of equations is derived which can be solved for the unknown coefficients.

$$\frac{\partial U_{total}}{\partial X_i} = 0 \Rightarrow \left[K_{ref} + \sum_i K_{patch_i}\right]\{X\} = \{F_t\} + \{F_E\} \quad \textbf{(5)}$$

where $\{F_T\}$ and $\{F_E\}$ are the generalized force vectors representing the thermal load and actuator force respectively. For further detail on the model, please see ref. [17].

2.2 Thermal Loading

The reflector moves in a geosynchronous orbit so its position relative to the sun, as well as the temperature distribution on the reflector surface changes. This distribution can be approximated by a bulk temperature shift of the entire reflector, combined with a linear temperature gradient. The temperature is modeled according to Eq. (6) , where T_0 is the bulk temperature shift at the center and ΔT is the linear temperature gradient across the reflector with respect to the temperature at the center. This temperature profile approximately captures the change in temperature that will be seen on the reflector at different points through its' orbit.

$$T(r,\theta) = T_0 + \Delta T \frac{r}{2a}\cos\theta \quad \textbf{(6)}$$

A graphical representation of this equation is shown in Figure 2, which shows the parameters used as well as how the temperature change is applied to the reflector.

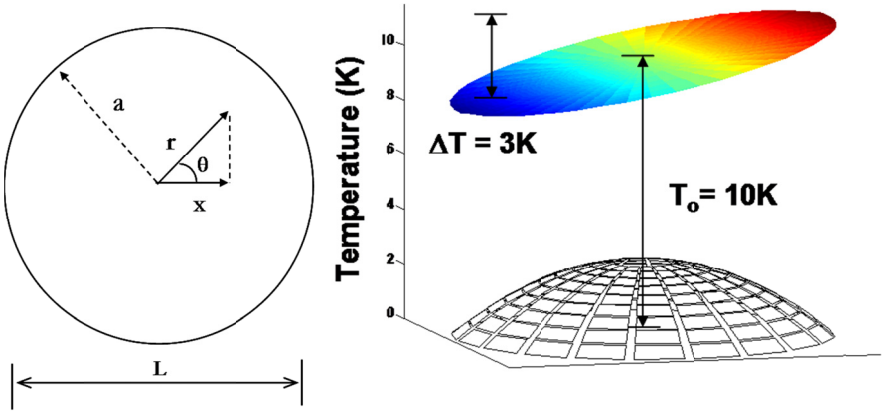

Figure 2 Illustration of parameters used in modeling temperature distribution.

2.3 Least Squares

Recall that the general form of the reflector/actuator system is given in Eq. (5). Furthermore, $\{F_E\} = [B_u]\{U\}$, where $\{U\}$ is a vector of the input voltages applied to each PVDF patch actuator and B_u is the corresponding control input distribution matrix. For control purposes, we are only interested in the transverse surface displacements, so a vector of surface transverse displacements $\{Y\} = [C]\{X\}$ is used. The matrix $[C]$ transfers the transverse Bessel coefficients to a rectangular grid of sensors, which are measured as $\{Y\}$. This vector can be considered the sum of two parts, as written in Eq.(7).

$$\{Y\} = \{Y_0\} + \{Y_E\} = [C]\left[K_{sys}\right]^{-1}\{F_T\} + [C]\left[K_{sys}\right]^{-1}[B_u]\{U\} \quad \textbf{(7)}$$

In this equation, $\{Y_o\}$ is a vector of sensor measurements representing the shape error due to the thermal loading, and $\{Y_E\}$ is the vector of sensor measurements as a result of only the patch actuator inputs.

The algorithm used to determine the optimal electric fields for a given patch configuration and loading/ shape error is the reflective Newton method [19]. The PVDF material can retain its piezoelectric properties only up to a certain value of the electric field. Beyond this value, it gets depoled (loses its piezoelectric properties). This threshold value determines the bounds on the electric field in the algorithm. The objective function, $J = \{Y\}^T\{Y\}$ is minimized in the least-squares sense, keeping the electric fields within the selected bounds.

3. MODEL VERIFICATION

Throughout this study, two distinct test beds are used. The first, a 2.4 meter diameter reflector, has been built to compare the analytical model developed above with an actual reflector. This reflector was built by ManTech NeXolve Technologies, and the PVDF actuators were attached at the Jet Propulsion Lab (JPL). The second test-bed used in this study is a 35 meter diameter model which conforms to desired attributes of the NASA NEXRAD reflector. This test-bed is used to show the efficacy of the algorithms of this study. The relevant geometric properties for both test-beds are given in Table 1 while the material properties, which are assumed to be the same for both test-beds, are listed in Table 2.

Table 1. Geometric properties of 2.4 meter test-bed and 35 meter test-bed.

Parameter	Description	2.4 Meter Test-bed	35 Meter Test-bed
R	Radius of Curvature	1.45 m	56 m
a	Planform Radius	1.2 m	17.5 m
h_{ref}	Thickness	50 μm	50μm

Table 2. Material properties for both 2.4 meter test-bed and 35 meter test-bed.

Parameter	Description	Value
ρ_r	Reflector Density	1420 kg/ m^3
E_r	Reflector Elastic Modulus	2.5 GPa
υ_r	Reflector Poisson's Ratio	0.34
α_{CTE}	Coefficient of Thermal Expansion	0.4 x 10^{-6} K^{-1}
ρ_a	Actuator Density	1780 kg/ m^3
E_a	Actuator Elastic Modulus	2.27 GPa
υ_a	Actuator Poisson's Ratio	0.225
h_a	Actuator Thickness	65 μm
d_{31}	Piezoelectric Constant	15x10^{-12} m/Volt
d_{32}	Piezoelectric Constant	6x10^{-12} m/Volt
V_{max}	Maximum Allowed Voltage	2000 V

For the 2.4 meter test-bed, a total of 168 rectangular PVDF actuators were attached to the surface of the reflector. These actuators are 2 cm wide by 27 cm long and were arranged on the reflector surface in three rings, as shown in Figure 3a. There are two types of actuators on the surface. All actuators on the left half of the reflector are normal PVDF actuators, while those on the right side of the reflector are 'double' actuators; one actuator is attached directly on top of another, which give twice the output of a single actuator. The lines that extend out of the reflector surface area here are the

flexible circuits used to take power to each actuator. The white dots seen in Figure 3b are the photogrammetry points used to measure the surface.

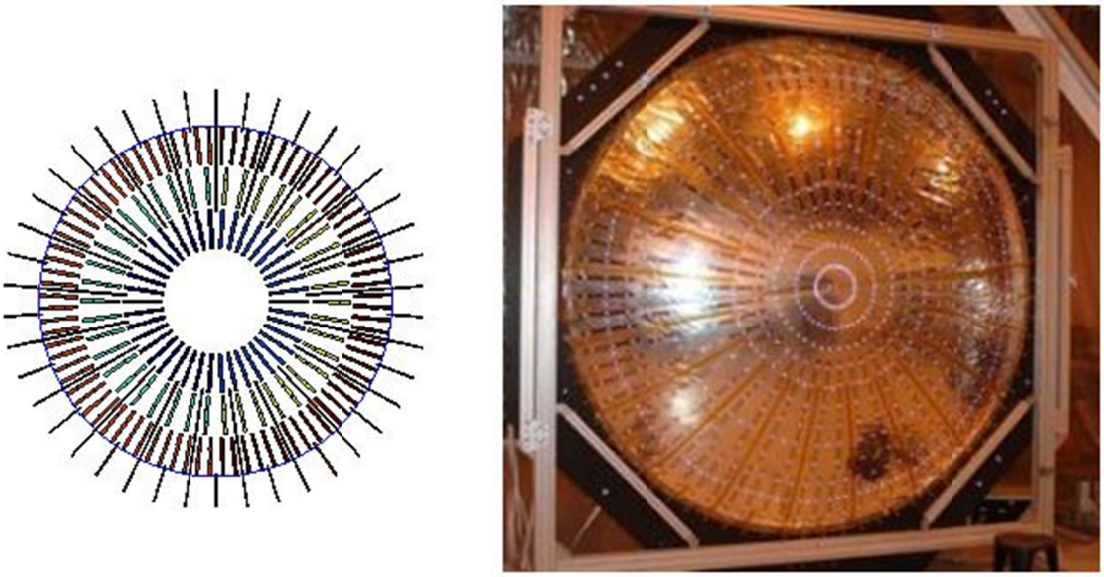

a) *b)*

Figure 3 Actuator placement on 2.4 meter reflector. *a*) shows analytic placement, while *b*) shows actual reflector.

The following figures (Figure 4 - Figure 6) show the analytical and experimental displacement results for varying powering scenarios. The analytical results are on the left, while the experimental results, obtained from the JPL reflector, are on the right. The out-of-plane displacement is measured in millimeters. Figure 4 shows the analytical and experimental displacement results for the case when the single actuators are powered with 1000 volts. Similarly, Figure 5 shows the displacement when 1000 volts is applied to only the double actuators. Finally, Figure 6 shows the out-of-plane displacement when all actuators are powered to 1000 volts.

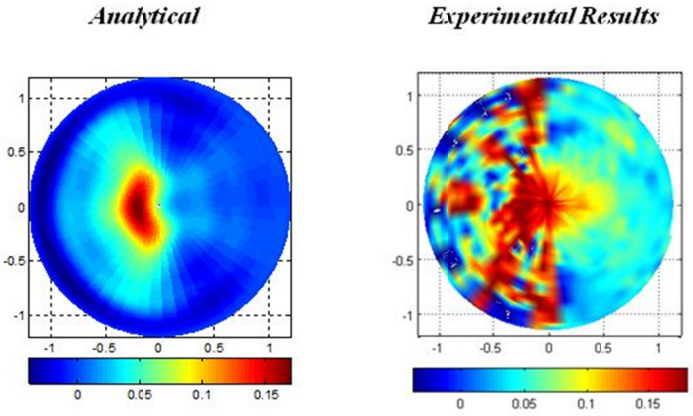

Figure 4 Comparison between the analytical and experimental model when 1000 V is applied to all SINGLE actuators. Displacement is in mm.

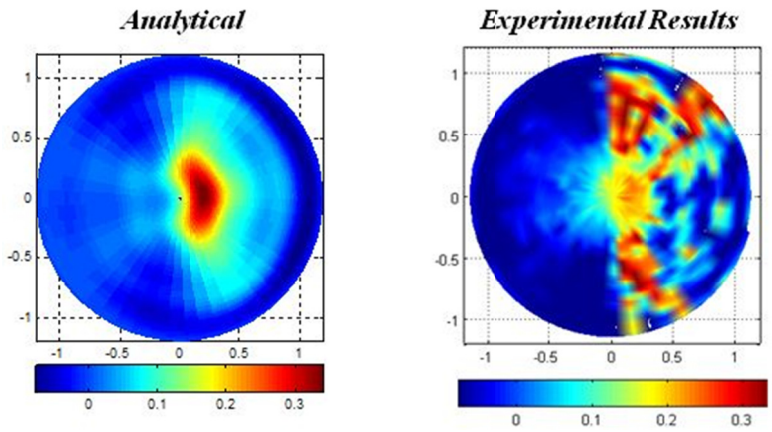

Figure 5 Comparison between the analytical and experimental model when 1000 V is applied to all DOUBLE actuators. Displacement is in mm.

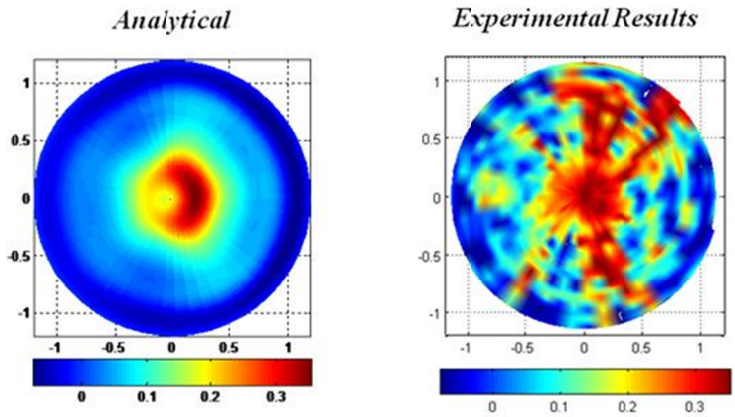

Figure 6 Comparison between the analytical and experimental model when 1000 V is applied to ALL actuators. Displacement is in mm.

While there is some discrepancy between the analytical and experimental results in these cases, the general magnitude is correct, as well as the overall movement trend. It does appear that some of the actuators create a larger displacement on the surface then do others. One possible explanation is that the actuators themselves are not perfectly bonded to the reflector. Many photogrammetry points are located directly on the actuators, so the photogrammetry system will read the movement of the actuator to which it's attached and not the actual reflector. If the actuator is not fully attached to the surface, then the surface will not move as much as the actuator, causing the photogrammetry measurement at that point to be incorrect. Even with these errors, there is good correlation between the general magnitude of the model and experimental results, as well as the general movement trend.

4. SIMULATION RESULTS

Results are given for the case of a 35 meter reflector when there is a surface error caused by a temperature change of the reflector surface. It is assumed there are 128 actuators divided into 8 rings, and 16 rays, which entirely cover the surface of the reflector. The first case, given in Figure 7, shows the reflector with a uniform temperature shift of $T_0 = 40$ K. On the left is the surface error of the reflector without any control, while the middle plot shows the surface error of the reflector after the least squares control is applied. The plot on the right shows the voltage applied to each actuator patch, where the patch number starts with 1 at the center and circles around to the outside edge. As shown, the RMS error is reduced from 0.88 mm to 0.09 μm, a reduction of 99.9%.

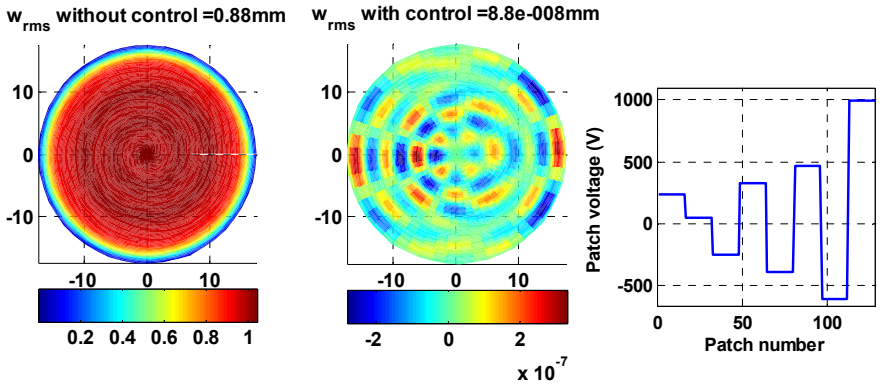

Figure 7 Graphical result for 35 meter reflector, 100% coverage, given a uniform temperature shift, T_0 = 40 K. All displacements are in mm.

The second case, Figure 8, illustrates the application of the control law to correct the shape error caused by a gradient temperature shift ΔT of 40 K, while T_0 is kept at 0 K. The RMS error is reduced from 0.28 mm to 0.8 μm, a reduction of 99.9%.

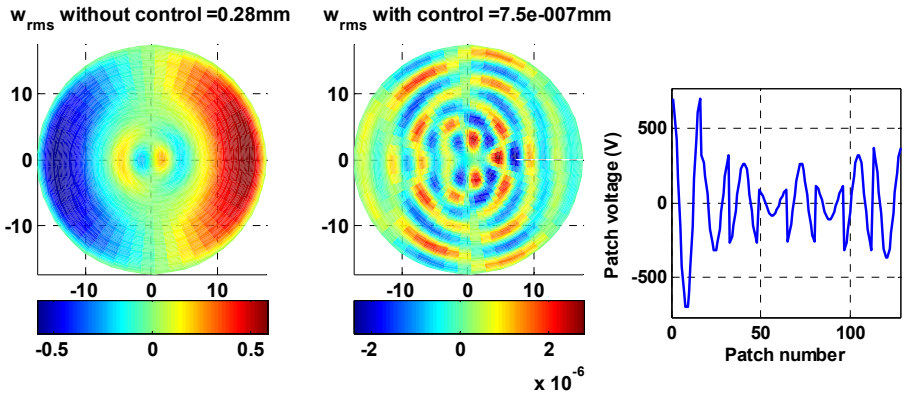

Figure 8 Graphical result for 35 meter reflector, 100% coverage, given a gradient temperature shift, ΔT = 40 K. All displacements are in mm.

The third case is a combination of the first two cases. A uniform temperature shift, T_0, of 40 K is applied with a gradient temperature shift ΔT of 40 K, as seen in Figure 9. In this case, the maximum applied temperature is 80 K, where the two temperatures are added together. The uncontrolled RMS error is 0.93 mm, while after the control the RMS error is reduced to 0.2 μm, or a reduction of 99.9%.

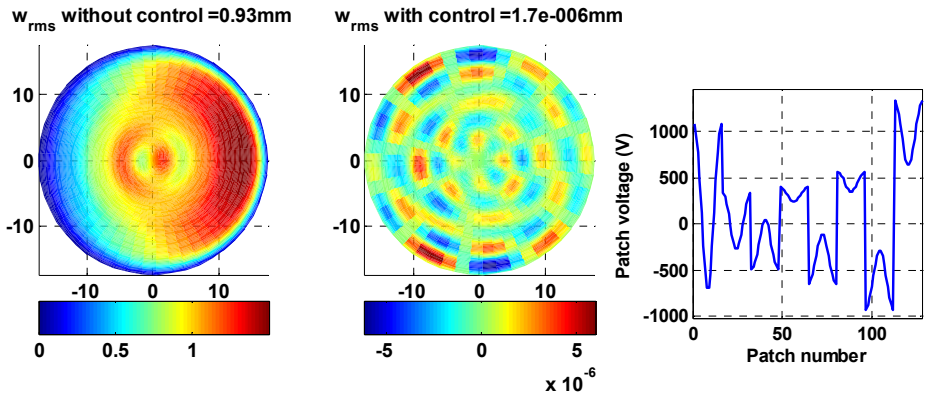

Figure 9 Graphical result for 35 meter reflector, 100% coverage, given a gradient temperature shift, ΔT = 40 K and a uniform temperature shift, T_0 = 40 K. All displacements are in mm.

These results show that given full surface coverage, accurate control of the surface is possible using PVDF actuators. The previous results assume that we have sufficient power supplies to control each actuator individually. While ideally each actuator should be controlled by an individual power supply, many times it is not realistically feasible due to design, weight, or cost constraints. There are many instances where the only solution is to group multiple actuators together and power each group with a single power supply. For best performance, the grouping of actuators must be optimized.

5. EME ALGORITHM

5.1 Explanation of EME Algorithm

The En Masse Elimination (EME) algorithm has been shown to be effective at finding the global optimal grouping for actuators, without having to test every possible grouping, as an exhaustive search would require [20]. The basic premise of the EME method is that by temporarily relaxing the power supply constraint, the resultant objective function measurement (RMS error) is a lower bound for multiple possible actuator combinations, which can be used to eliminate large areas of the design space. While the EME algorithm is still an exponential algorithm similar to the exhaustive search, large numbers of iterations can be eliminated without testing each possibility. A flowchart of the EME process is given in Figure 10 and a step by step process of the method is given below.

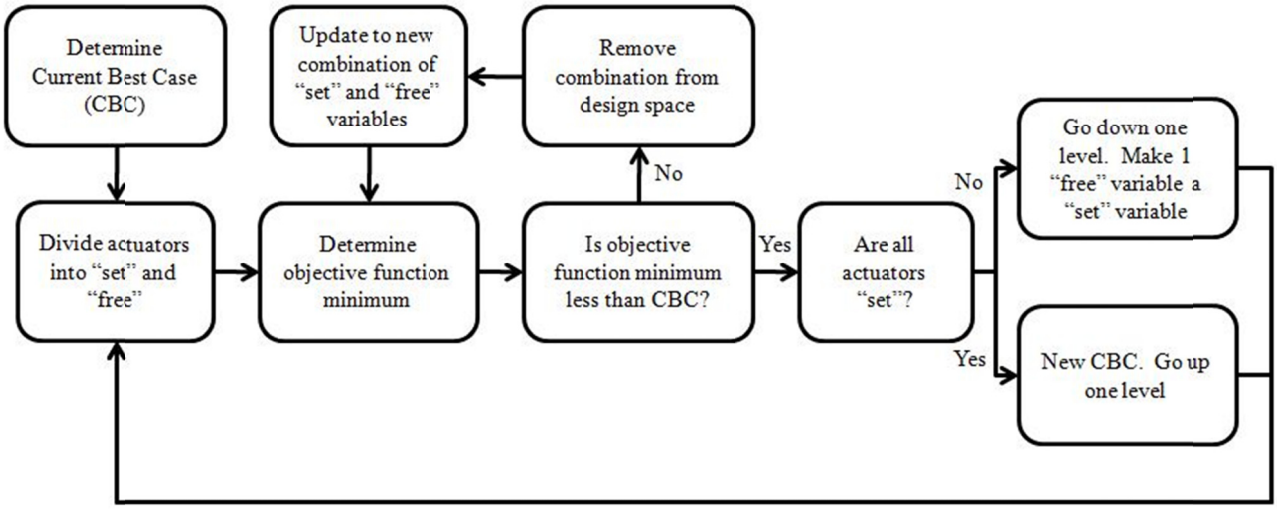

Figure 10 Flowchart for basic EME algorithm

To start the EME algorithm, a baseline value of the minimized RMS error must be found where all power supply constraints are satisfied. Using a quick heuristic algorithm or simply choosing a case at random, we determine an initial grouping and calculate the RMS error. This design is called the Current Best Case (CBC). The results from the EME algorithm are always compared to the CBC value to determine which grouping of actuators can be eliminated.

During each iteration of the EME algorithm, the actuators are divided into two distinct groups: first, some actuators are "set", meaning that they are grouped to the given power supplies. Second, we allow some actuators to be "free", meaning they are not grouped together, but are connected to additional individual power supplies. These extra power supplies are not counted towards the power supply constraint. Let us take, for example, a system with three power supplies and fifteen actuators. We can have ten "set" actuators, connected to the three power supplies. Then we allow the remaining five actuators to be "free" by connecting them to their own individual power supplies, relaxing the power supply constraint from three to eight power supplies. This allows the "free" actuators to take on any voltage value instead of being forced to take on only the voltage value of a group. For each iteration of the EME algorithm, the "set" actuators are placed into a given grouping, where the number of groupings is constrained by the number of power supplies available. The "free" actuators are each connected to individual power supplies. Using this combination of "set" and "free" actuators, the RMS error is then calculated. It is at this point in the algorithm that large areas of the design space can be removed. The minimized RMS error is the lower bound for any actuator groupings that have the same combination of "set" actuators as in this specific case. If the RMS error calculated is greater than the RMS error of the CBC design, then regardless of which group each "free" actuator could be placed in, the minimized RMS error will always continue to be greater than this lower bound. Therefore, every grouping that has this combination of "set" actuators can be removed from consideration.

The basic EME algorithm runs through each possible combination iteratively, attempting to remove the largest amount of the design space possible. It starts by setting the majority of the actuators to be "free". If the minimized RMS error is larger than the RMS error of the CBC design, multiple design possibilities can be removed, the algorithm updates to a new combination of "set" variables, and another iteration is run. If, on the other hand, the minimized RMS error is less than that of the CBC design, no new knowledge is gained and no designs can be removed. Under this condition, if all the actuators are "set", meaning the design is now feasible, a new CBC has been found. If not all actuators are "set", one "free" actuator is placed into a group and becomes "set". The RMS error is again minimized using the new grouping configuration and is again compared to the RMS error of the CBC design. As more actuators become "set", the probability that we can remove some actuator groupings is increased, though the number of actuator groupings that can be removed during each iteration becomes smaller.

The EME algorithm is stopped once every possible grouping combination has either been tested or removed from the design space. In this way, the global optimal solution is guaranteed to be found, without the need for an exhaustive search of each possible combination.

5.2 EME Algorithm Results

In this section, we illustrate how particular cases of error are corrected by the application of the EME algorithm on the reflector. The results shown are for the case of a 35 meter reflector, assuming 32 actuators divided into 4 rings and 8 rays, which entirely cover the surface of the reflector. A constraint of 4 power supplies is enforced on the reflector. The first case is given in Figure 11, which shows the reflector with a uniform temperature shift, T_0, of 40 K. On the left is the surface error of the reflector without any control, while the middle plot shows the surface error of the reflector after the EME algorithm is used to determine the actuator grouping and the least squares control is applied. The plot on the right shows the voltage applied to each actuator. As shown, the RMS error is reduced from 0.99 mm to 0.36 mm, a reduction of 64%.

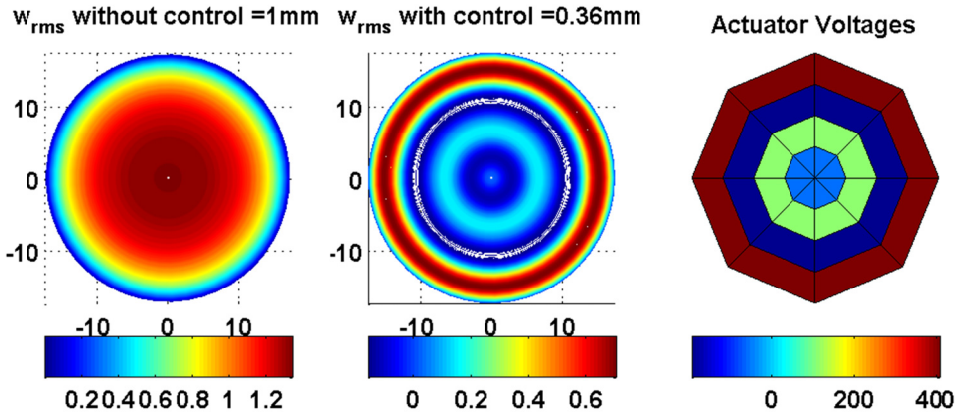

Figure 11 Graphical result for 35 meter reflector, 100% coverage, and 4 power supplies, given a uniform temperature shift, T_0 = 40 K. All displacements are in mm.

The second case, Figure 12, illustrates the application of the EME algorithm and control law to correct the shape error caused by a gradient temperature shift ΔT of 40 K, while T_0 is kept at 0 K. Again, the EME algorithm determines the optimal grouping assuming 4 power supplies, and then the least squares control is applied to the groups. The RMS error is reduced from 0.24 mm to 0.099 mm, a reduction of 58.8%.

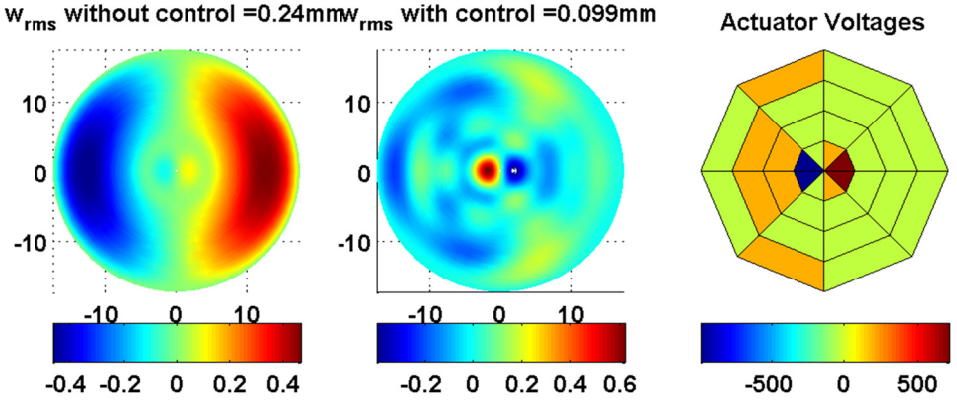

Figure 12 Graphical result for 35 meter reflector, 100% coverage, and 4 power supplies, given a gradient temperature shift, ΔT = 40 K. All displacements are in mm.

The third case is a combination of the first two cases. A uniform temperature shift, T_0, of 40 K is applied with a gradient temperature shift ΔT of 40 K, as seen in Figure 13. In this case, the maximum applied temperature is 80 K, where the two temperatures are added together. The EME algorithm is used to determine the optimal grouping, and the least squares control is used to determine the optimal voltages for each grouping. The uncontrolled RMS error is 1.00 mm, while after control the RMS error is reduced to 0.37 mm, or a reduction of 63%.

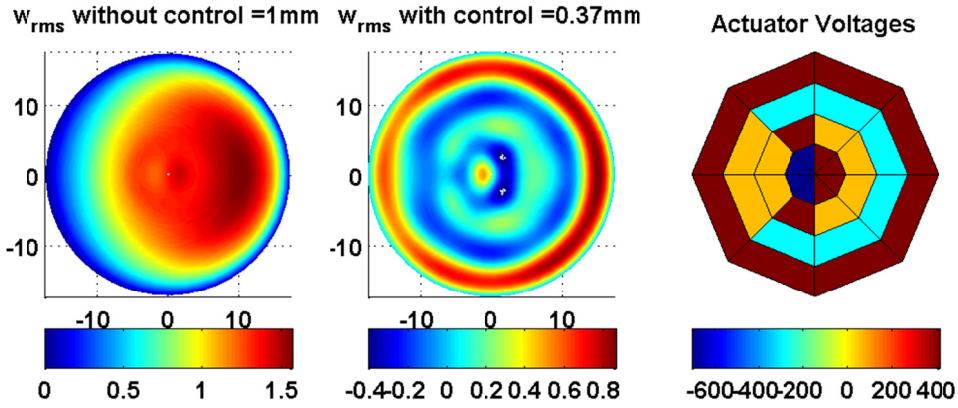

Figure 13 Graphical result for 35 meter reflector, 100% coverage, given a gradient temperature shift, ΔT = 40 K and a uniform temperature shift, T_0 = 40 K. All displacements are in mm.

Table 3 shows the total number of iterations required for the EME algorithm to search the entire design space and guarantee the global optimal solution. For 32 actuators and 4 power supplies, the total number of possible combinations is greater than $1.8e^{19}$. Even for the case of $T_0 = 40$ K, $\Delta T = 40$ K, where the total number of iterations required by the EME algorithm is close to 200 million, this is still a drastic reduction from an exhaustive search method.

Table 3. Iterations required for EME convergence.

T_0	ΔT	Number of Iterations
0 K	40 K	17,505,322
40 K	0 K	887,039
40 K	40 K	196,730,884

6. CONCLUSION

A comprehensive reflector/actuator model has been developed for a highly flexible space reflector. This model has been experimentally verified using a 2.4 meter Kapton reflector with 168 PVDF actuators attached to the surface. While the analytical model does not perfectly match the experimental work, there is good correlation between the general magnitude of the model and experimental results, as well as the general movement trend.

Using the analytical model, results are found for a 35 meter reflector. These results show that the surface of a reflector that is fully covered with PVDF actuators can be controlled to tight tolerances. In addition, analytical results have been given for a fully covered reflector with a constraint on the number of power supplies available. Utilizing the En Masse Elimination technique, the optimal grouping configuration was found without resorting to an exhaustive search of every possible configuration.

7. ACKNOWLEDGMENTS

The work described was performed at University of Michigan and Jet Propulsion Laboratory, California Institute of Technology under a contract with the National Aeronautics and Space Administration.

REFERENCES

[1] Ruggiero, E., and Inman, D., "Gossamer Spacecraft: Recent Trends in Design, Analysis, Experimentation, and Control, J. of Spacecraft and Rockets, Vol. 43(1), 10-24 (2006).

[2] Im, E., Durden, S.L., Rahmat-Samii, Y., Fang, H., Cable, V., Lou, M., and Huang, J., "Advanced Geostationary Radar for Hurricane Monitoring and Studies," Proc. IEEE Radar Conference, 307-311 (2004).

[3] Im, E., and Durden, S.L., "Instrument Concepts and Technologies for Future Spaceborne Atmospheric Radars," Proc. SPIE Enabling Sensor and Platform Technologies for Spaceborne Remote Sensing, 5659, 61-72 (2005). doi: 10.1117/12.579066.

[4] Haftka, R. T., and Adelman, H. M., "An Analytical Investigation of Shape Control of Large Space Structures by Applied Temperatures," AIAA Journal, Vol. 23, 450-457 (1985).

[5] Lindler, J. and Flint, E., "Boundary Actuation Shape Control Strategies for Thin Film Single Surface Shells," Collection of Technical Papers AIAA Structures, Structural Dynamics and Materials Conference, Vol. 5, 3360-3370 (2004).

[6] Jenkins, C.H. and Marker, D.K., "Surface Precision of Inflatable Membrane Reflectors," ASME Journal of Solar Energy Engineering., Vol. 120, 298-305 (1998).

[7] Tabata, M. and Natori, M., 1995, "Active Shape Control of a Deployable Space Antenna Reflector," Sixth International Conference on Adaptive Structures, 177-187 (1995).

[8] Jenkins, C. and Schur, W., "Gore/Seam Architectures for Gossamer Structures," Journal of Spacecraft and Rockets, Vol. 39(5), 298-305 (2002).

[9] Coleman, T. F. and Li, Y., "A Reflective Newton Method for Minimizing a Quadratic Function Subject to Bounds on Some of the Variables," SIAM Journal of Optimization, 6, 1040-1058 (1994).

[10] DeSmidt, H. A., Wang, K. W. and Fang, H., "Optimized Gore/Seam Cable-Actuated Shape Control of Gossamer Reflectors," Journal of Spacecraft and Rockets, Vol. 44(5), 1122-1130 (2007).

[11] Pattom, M., "High Precision Shape Control of Large, Light Weight Space Reflectors," Master Thesis, Mechanical and Nuclear Engineering Dept., The Pennsylvania State University, University Park, PA (2006).

[12] Rader, A. Yousefi-Koma, A., Afagh, F., and Zimcik, D., "Optimized Grouping of Piezoelectric Actuators on a Flexible Fin," Proceedings of SPIE, 5762, 123-131 (2005).

[13] Grewal, A., and Tse, D., "Optimization of Piezoelectric Actuator Grouping for Aircraft Cabin Noise Control," Collection of Technical Papers–AIAA/ASME/ASCE/AHS/ASC Structures, Structural Dynamics and Materials Conference, 2, 135-149 (2000).

[14] Grocott, S., Dynamic Reconstruction and Multivariable Control for Force-actuated, Thin Facesheet Adaptive Optics," PhD Thesis, Department of Mechanical Engineering, Massachusetts Institute of Technology, Cambridge, MA (1997).

[15] Jamoom, M., Feron, E., and McConley, M., "Optimal Distributed Actuator Control Grouping Schemes," Proc. of the 37th IEEE Conference on Decision and Control, Vol. 2, 1500-1505 (1998).

[16] Lin, C., "Towards Optimal Strain Actuated Aeroelastic Control," PhD Thesis, Department of Mechanical Engineering, Massachusetts Institute of Technology, Cambridge, MA (1996).

[17] Fang, H., Pattom, M., Wang, K., and Im, E., "Shape Control of Large Membrane Reflector with PVDF Actuation," Collection of Technical Papers–AIAA/ASME/ASCE/AHS/ASC Structures, Structural Dynamics and Materials Conference, 2, 1653-1663 (2007).

[18] Soedel, W., Vibrations of Shells and Plates 2nd ed., Marcel Dekker, New York (1993).

[19] Coleman, T. F. and Li, Y., "A reflective Newton method for minimizing a quadratic function subject to bounds on some of the variables," SIAM J. of Optimization, 6, 1040-1058 (1994).

[20] Hill, J. R. and Wang, K., "On the Development of the En Masse Elimination Algorithm for Actuator Grouping Optimization in Adaptive Structures," ASME Conf. on Smart Materials, Adaptive Structures and Intelligent Systems (2010).